Article

Sheet Metal Design Approach for 3D Shaped Facade Elements with Integrated Solar Thermal Functionality

Peter Scholz [1,*], Dieter Weise [1], Linda Schmidt [2], Martin Dembski [2], Alexander Stahr [2], Martin Dix [1], Florin Duminica [3], Sebastien Le Craz [3] and Jiri Koziorek [4]

[1] Department of Sheet Metal Forming, Fraunhofer Institute for Machine Tools and Forming Technology, 09126 Chemnitz, Germany

[2] Hochschule für Technik, Wirtschaft und Kultur Leipzig HTWK, 04277 Leipzig, Germany

[3] Department Advanced Surface and Smart Solutions, CRM Group, 4000 Liege, Belgium

[4] Department of Cybernetics and Biomedical Engineering, VSB—Technical University of Ostrava, 70800 Ostrava, Czech Republic

* Correspondence: peter.scholz@iwu.fraunhofer.de

Abstract: This paper provides an overview of the development of a 3D formed and metal-based facade element that combines a custom design and solar thermal functionality. To achieve this, a novel simplified solar thermal collector structure was developed using formed sheet metal half-shells with an integrated channel structure on the inside and a special absorber coating on the outside. The sheet metal half-shells were manufactured by highly innovative incremental sheet forming (ISF), which allows seamless integration into existing facades. As a part of this paper, the initial test results on thermal efficiency and the energy accumulation of the new collector type are presented.

1. Introduction

The reduction of harmful greenhouse gases is one of the biggest challenges of our time. The use of unlimited available solar thermal power as renewable energy can help to support efforts to reduce CO_2 emissions worldwide. More than 40% of the total energy consumption in Europe can be allocated to heating, hot water, and illumination [1]. This corresponds to almost 20% of the total CO_2 emissions. Especially in the building industry, reducing CO_2 emissions is one of the main drivers. By using modern building envelopes, the required energy for heating and cooling can be minimized [2]. The major goal is the realization of affordable zero-energy buildings. One effective way of achieving these objectives is the use of solar thermal energy. The solar radiation at our latitudes is perfectly suited for thermal use.

In central Europe, solar radiation produces, on a 1 m^2 area, 1000 kWh/year to 1100 kWh/year [3], which is equivalent to 100 L of fuel oil or 100 m^3 of natural gas. For this reason, the building sector has a strongly growing interest in facade-integrated solar thermal absorbers, which shall be presented in this paper.

A broad range of solar thermal collectors have been available on the market for decades worldwide. These products are credible and generally made to a high technical standard, especially in Europe with a homogeneous market. However, there is a shortage in the field of solar thermal products that are suited for building envelope integration to create high-quality architecture [4,5]. Functional and constructive aspects, together with aesthetics, have to be considered. State-of-the-art solar thermal collectors are not flexible in shape and size due to the hydraulic fluid circuits fixed to solar absorbers. Architectural requests for design freedom require the hydraulic system concept to be redesigned, which is generally difficult and expensive for conventional means of production. Conventional production methods for absorbers limit the flexibility in collector design [6] and such a lack

of flexibility significantly reduces the potential application of solar thermal systems [7]. The production of solar collectors in sheet metal half-shell design by means of hydroforming was investigated in the European Union (EU) project with the acronym "BIONICOL" [8] and in "Industrielle Gemeinschaftsforschung" (IGF) project No. 339 ZN [9]. However, curved surfaces cannot be obtained with the shown technologies and the channel structures can only be manufactured on both sides, which has a disadvantageous effect on the design freedom of the facade. The integration of flat-plate solar thermal collectors is only possible for opaque envelopes (roofs and facades) so far [10]. The structure of evacuated tubes allows mounting on transparent envelopes as sun shading, but this kind of application is rare. The application potential of incremental sheet forming (ISF) in solar absorbers was demonstrated in [11] by the production of absorber lamellae using incremental forming technology.

The thickness of solar collectors affects their integration, especially for facades. Thick solar thermal collectors are difficult to implement as functional elements or as sun shading. The appearance of solar collectors is affected by the glass (glazed collector) and absorber surface treatment. State-of-art collectors apply highly transparent, low-iron glass for glazing and black or dark-blue spectrally selective coatings with high absorptance (0.95) and low emittance (0.05). Solar collectors integrated into facades are more conspicuous than collectors installed on rooftops. Many studies and surveys have shown that architects prefer a large variety of absorber colors [12], and they even regard the possibility of a custom color choice as essential. Manufacturers can meet the demand for a variety of absorber colors by means of solar paint coatings, but such collectors show considerably reduced thermal performance compared with quality selective coatings in the usual solar collectors commercially available in Europe [13].

This paper presents a new design of a solar thermal collector. The focus of this paper is fabrication with ISF, concepts for integration into facade systems, possible design arrangements, and the development of the absorber coating. Furthermore, initial results on the thermal efficiency and performance of the new collector type are presented and evaluated.

2. Materials and Methods

2.1. Principal Collector Design

Figure 1 shows the layout of the developed collector design, which consists of two layers of cold-rolled deep-drawing steel DC06 (t = 0.8 mm) joined together in a fluid-tight manner by laser welding.
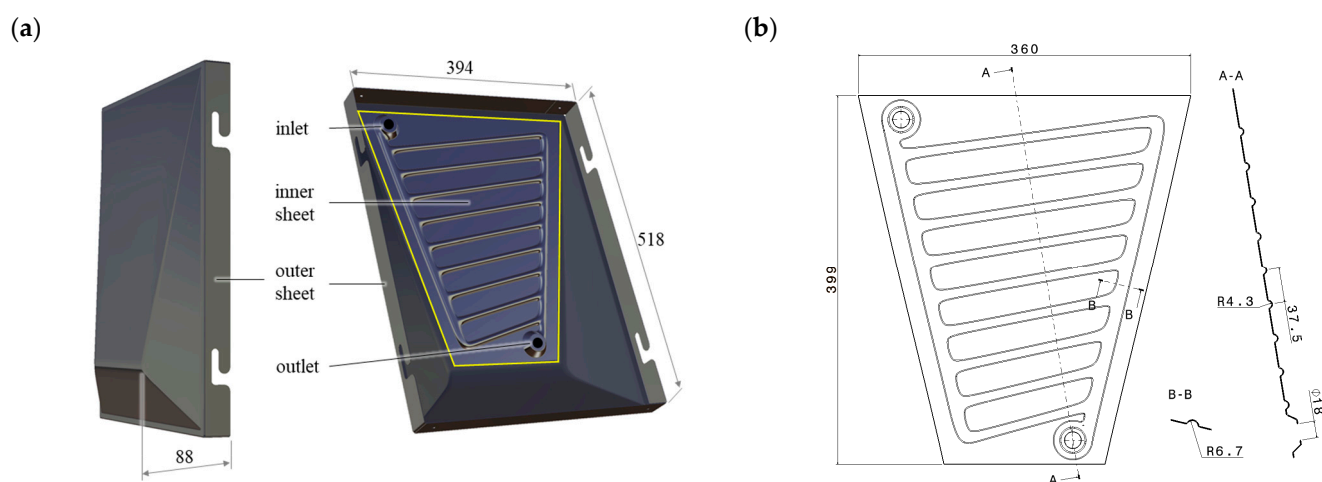

Figure 1. Principal collector design: (**a**) CAD model of the assembled collector and (**b**) drawing of the inner sheet with the channel structure.

The three-dimensional shaped outer sheet is designed as a closed cassette with integrated notches for hooking into the façade's substructure. To integrate the solar thermal functionality, the flat inner sheet has a two-dimensional channel structure and is attached to the outer sheet. The use of this simple geometry for the inner sheet ensures a good fit between the two components, which is essential for the joining process. The channel structure chosen was a harp structure, which has also been used in commercially available flat plate collectors. With this structure, the area to be cooled can be efficiently passed through with low pressure loss at the same time. For hydraulic connection, parallel planar surfaces were proposed in the inlet and outlet areas for the easy integration of conventional fittings.

The representative design of the geometry of the exterior sheet was determined by the results of the solar gain analysis, the architectural design boundaries, and the constraints of the forming process, which are described in the following sections.

2.2. Architectural Aspects and Facade Integration

2.2.1. Necessity of Research into Solar Thermal Facade Elements in Architecture

Endeavoring to be part of the solution, the publicly funded research project "FutureFacade" strives to do its part for climate protection in the construction industry by utilizing the inextricable connection to resource and energy efficiency. The integration of solar thermal energy into facades holds great potential for generating solar yields that have, so far, remained largely untapped. Although a study by the Leibniz Institute for Ecological and Regional Development (IÖR) shows that a total of 12,000 km^2 of facade area in Germany can be used for solar energy, no architecturally sophisticated solar thermal facade elements exist yet [14,15]. The combination of solar thermal energy with inner-city building surfaces can be used for domestic hot water, heating support, and cooling. Regarding unforeseeable developments in the cost of all fuels, solar thermal energy offers a sustainable and cost-effective alternative.

2.2.2. Architectural Innovation

While conventional collectors are visually recognizable by the glass and the dark-blue absorber surface, more complex appearances can be created using mono-material panels made of metal. Hence, through innovating solar modules, a novel structure was created in this project. Linking architectural aspiration and sustainability was paramount. The functional integration, which was not visible on the outside, was achieved by two combined sheet metal panels invisibly welded together.

2.2.3. Design Criteria for the Collector Geometry based on Solar Thermal Aspects

Optimizing the geometry of the outer panel was most important in order to adapt the modules as efficiently as possible to the irradiation conditions using site-specific weather data while also taking into account the manufacturing constraints (e.g., maximum wall angle and minimal radius). The adjustment of the module geometry and, thus, the solar-active area and the irradiation angle was regulated by a digital parametric design tool. This allowed the yields to be controlled and optimized, which is a pioneering development in sustainable building construction.

The solar gain analysis showed that the chosen shape could provide 792 kWh/m^2 per year for a southern orientation using the Chemnitz, Germany, region as an example (Figure 2). Different rectangular-based shapes were tested throughout the project. The analysis showed that flat collectors had the lowest potential for solar gain. Plenty of design studies have been conducted. Round, triangular, rectangular, and hexagonal formats were also tested as irregular freeform shapes. In the end, the final polygonal shape lent itself best to the chosen forming technique and the solar gains that were to be achieved. The rectangular base allowed standardized substructures to be used. The rather simple basic shape contained a lot of freedom in the arrangement and variation of the geometry as a pattern, ensuring that design freedom could be kept (Figure 3). Compared with the chosen

polygonal shape, there would be a loss of 165 kWh/m^2 per year. Round double-curved shapes had the best solar-gain effect (809 kWh/m^2 per year), but were excluded due to the manufacturing technique after some forming tests, as there was a large spring-back effect after forming. Therefore, the polygonal shape was optimal from all tested design studies (Figure 2).
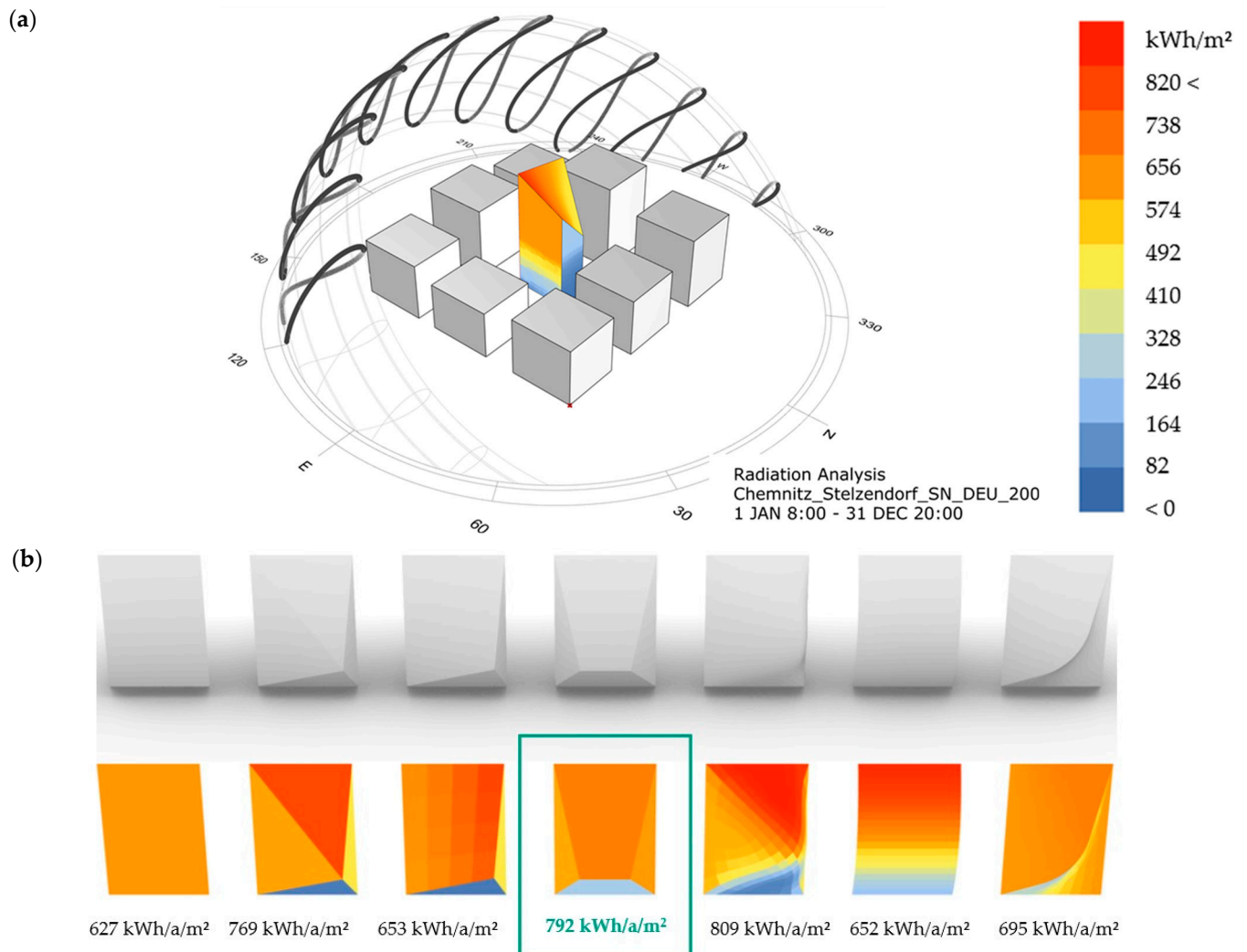
(**a**)

(**b**)

627 kWh/a/m²   769 kWh/a/m²   653 kWh/a/m²   **792 kWh/a/m²**   809 kWh/a/m²   652 kWh/a/m²   695 kWh/a/m²

Figure 2. Solar gain analysis (**a**) of different shapes (**b**) with a rectangular base performed with the energy-simulation engine EnergyPlus™ in combination with the Grasshopper plugin Ladybug for Rhinoceros® 3D.
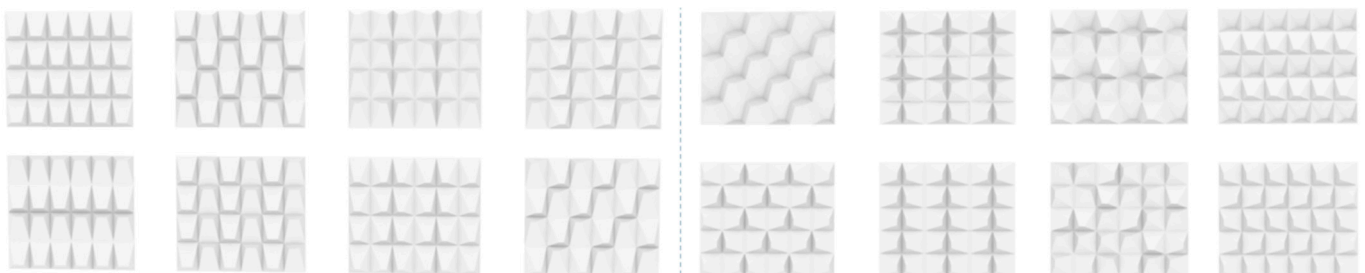

Figure 3. Variations and patterns of polygonal panels.

2.2.4. Facade Construction and Hydraulic System

The facade panel was designed as a simple standardized cassette and could thus be hooked into the bolt suspension. (Figure 4b). Owing to the standardized system used, it was possible to use facade (under-) constructions from various manufacturers. (Figure 4a). By using a standardized substructure, the effort required for assembly and maintenance can be decreased and the economic efficiency can be increased.
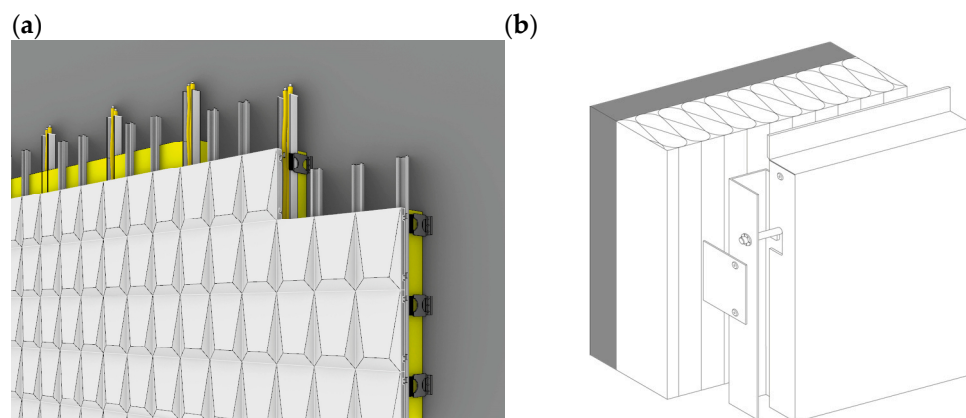

Figure 4. Visualization of facade construction (**a**) and under-construction detail (**b**).

The facade panel was a mono-material system. There was an outer panel and an inner panel welded together. The inner panel represented the channel structure, which was designed as a common harp shape. (Figure 5a) With regard to the most energy-efficient design of the fluid channels within the facade elements, computational fluid dynamics (CFD) simulations were carried out to achieve optimized performance for the facade element.
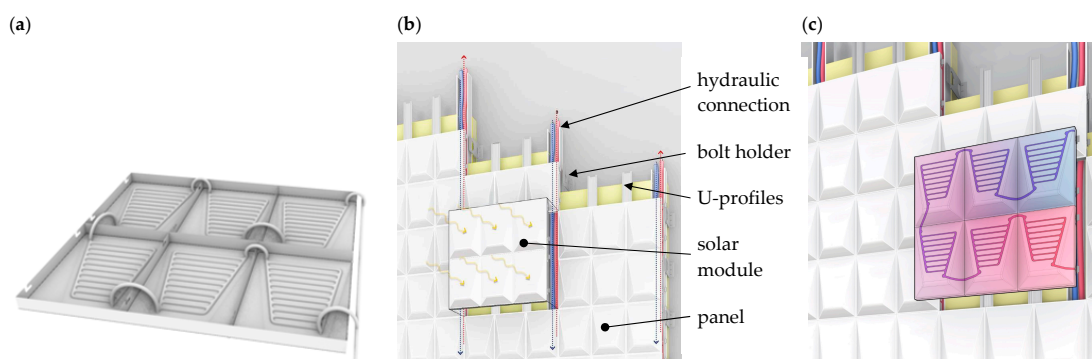

Figure 5. Schematic illustration of the addition of the panels (**a**), schematic illustration of facade construction (**b**), and schematic illustration of panel function (**c**).

To build a facade system that can operate as a power plant, the panels were connected in series and formed one module when connected in a mirrored position. (Figure 5c). One module at a time was then connected to the vertical cable routing. (Figure 5b). A pump ensured the circulation of the fluid in the facade. A heat exchanger provided the energy to the heating units, so the facade system became its own sustainable power plant to harvest renewable heat.

2.2.5. Architectural Results

The designed panel holds the potential to create new appearances for urban spaces and positively influence the use of renewable energy. (Figure 6) The panel can be used for new construction and existing projects. It can be used on large-scale installations in rural areas, as well as on urban facades, and thus has multiple applications. Therefore,

the project is a huge step in Mono-Material Design, facade design, architecture, and the building industry and renewable energies in general.
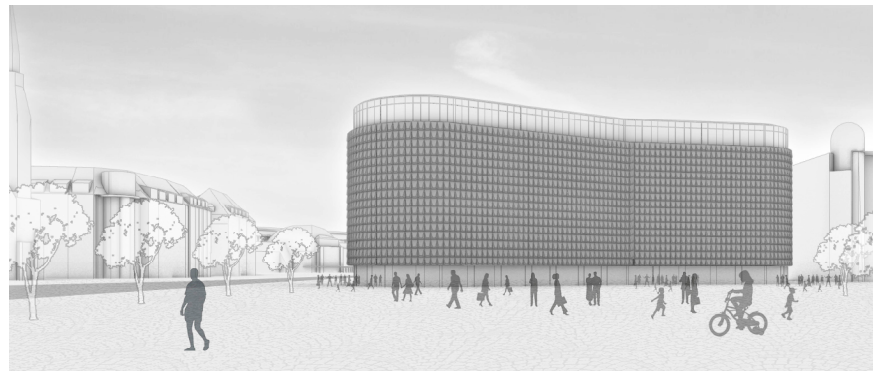

Figure 6. Visualization of a sample façade.

2.3. Demonstrator Manufacturing

2.3.1. Forming

For the manufacturing of the solar collector sheets, incremental sheet metal forming (ISF) in combination with subsequently performed bending operations (only for the outer sheet) was used. With ISF, the final part of the geometry is successively formed by the CNC-controlled movement of a forming stylus over a counter die (Figure 7a). In comparison with conventional forming methods (e.g., deep drawing), this reduces tool costs and the time required to achieve the first finished part.
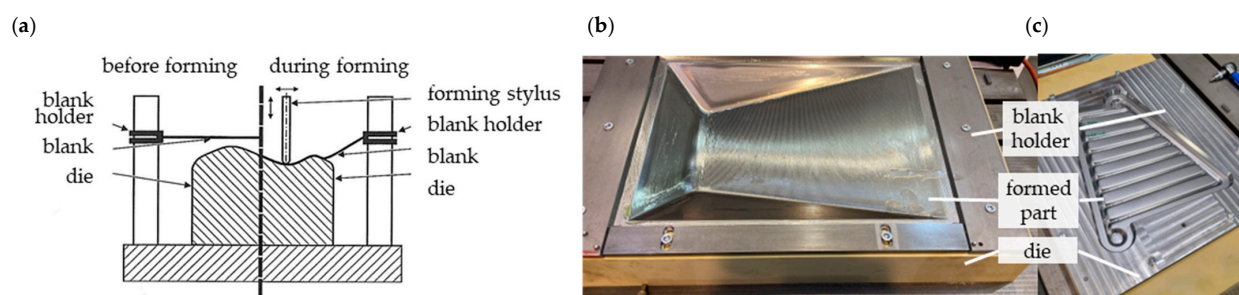

Figure 7. Incremental sheet forming: (**a**) process principle, (**b**) clamped outer sheet after forming, and (**c**) clamped inner sheet after forming.

For the forming of the test components, a polyurethane counter-die (material: obomodulan$^\circledR$ 1600 sand) was used, in which the cut-to-size sheets were clamped by means of a blank holder (Figure 7b,c). As a lubricant, Raziol CLF 125F was used for all forming trials.

To avoid wrinkling during forming, the outer sheet was formed in two steps. In the first step, a stylus diameter of 100 mm with a z-increment of 0.2 mm was used. In the second step, the final shape was formed with a stylus diameter of 6 mm and an increment of 0.2 mm. For both steps, a z-constant tool path in helix design was chosen, with a total forming time of approx. 2 h. After unclamping, the edges of the outer sheet were folded and mechanically joined at the corners to create the closed cassette design shown in Figure 1.

The shape of the inner sheet could be formed in one step with a forming stylus diameter of 6 mm, a z-increment of 0.2 mm, and a forming time of approx. 45 min, also by using a z-constant tool path in helix design. With these parameters, the inner and outer sheets could be successfully formed without failures. For both geometries, the global shape deviation was approx. 1 mm compared with the original CAD geometry which is within the common tolerances for facade panels.

2.3.2. Joining

A welding Nd:YAG laser of 3 kW mounted on a robot was used for the assembly of the inner and outer formed sheets. The experimental set-up is presented in Figure 8a. Specific tools were used to optimize the contact between the welded surfaces and to prevent gaps from forming between the steel sheets; otherwise, the upper sheet could be pierced by the laser beam. The first tool (Figure 8b) was developed to allow the welding of the outer contour of deformed panels, and the second one (Figure 8c) was designed for the welding of lines between the channels, allowing the passage of fluid through the drawn network and avoiding the swelling of the panels. Finally, the fluid connectors were fixed using manual tungsten inert gas (TIG) welding (Figure 8d).
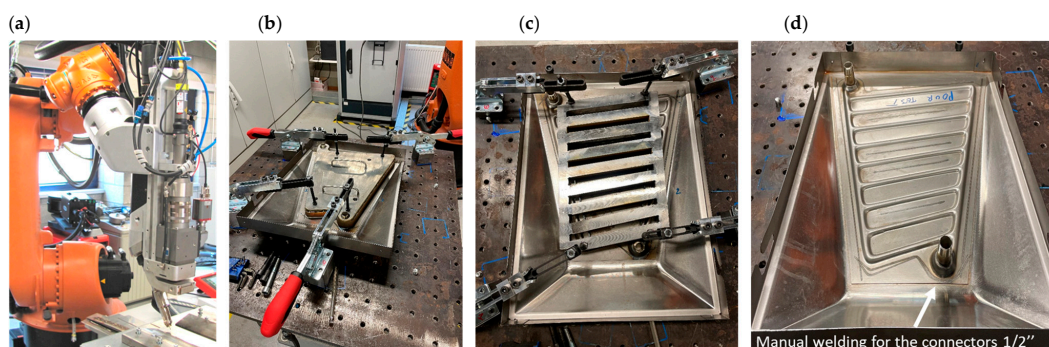

Figure 8. Laser welding setup: (**a**) laser head mounted on a robot, (**b**) clamped tool for outer contour, (**c**) clamped tool for inner channels; (**d**) TIG welding for fluid connectors.

Laser welding requires a compromise between the thermal load and the welding speed in order to limit damage to the outer sheet's steel surface. The laser beam must cross the top sheet and penetrate the bottom one without crossing it. Figure 9a shows a cross-section micrograph of the welding of two steel sheets. The focal spot is in the range of 0.8 mm to 1 mm for the following welding parameters: laser head speed of 3 m/min, steel sheet thickness of 0.8 mm, and laser power of 1.4 kW. Various parameters, such as the accuracy of the robot trajectory, the variation in the steel thickness generated by the incremental forming, as well as the distance between the steel sheets, can influence the welding beam penetration, leading to marks on the back side of the panel. Figure 9b (left) shows the impact of the welding beam on the back side of the panel. However, additional surface treatment, such as sandblasting, can remove the oxides generated by the laser beam overheating and can also considerably decrease the thermal stress near the welding lines. Figure 9b (right) shows the same surface as Figure 9b (left) after sandblasting.

A potential optimization requires an increase in the thickness of the back metal sheet to decrease the thermal effect and to increase the welding process parameters. However, for this project, the choice to simplify the assembly system drove the use of the same material and same thickness for both the inner and outer shaped steel sheets.
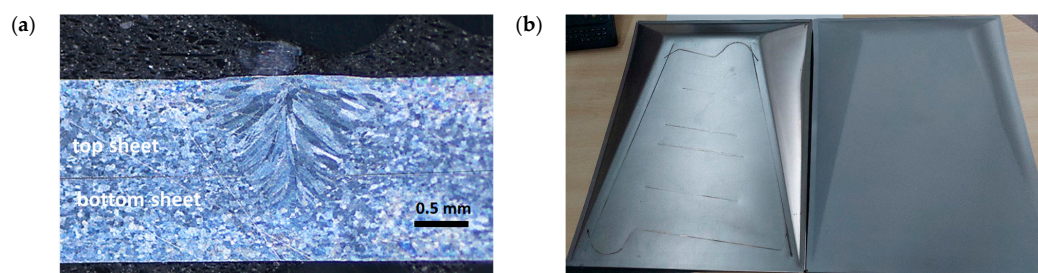

Figure 9. (**a**) Cross-section micrograph of the welding of two steel sheets and (**b**) welding lines on the front side of the panel: as initially welded (left) and after sand-basting (right).

2.3.3. Strategies and Concepts for Absorbing Coatings

The design of a non-glazed solar absorber for practical application requires the development of a robust coating applied by low-cost techniques. This coating must exhibit high absorption efficiency in the ultraviolet and visible regions of the solar radiation spectrum. Therefore, the reflectance should be minimized in these regions of the solar spectrum. Additionally, the loss of heat to the surroundings via convection or conduction should be reduced as much as possible. Thus, there are conflicting requirements for strong absorption in the solar spectrum, with minimum emission in the infrared range. The use of deep-drawing steel DC06 as a substrate requires additional corrosion protection. The outer formed steel sheet was protected by an 80 μm-thick aluminum coating deposited by the twin arc-wire thermal spray technique. The role of this additional coating is to prevent steel corrosion in case of surface scratches during the manipulation of the panels. Thermally sprayed aluminum, in combination with organic and ceramic coatings, is a common method used for corrosion protection for bridges, ships, and oil and gas installations. These systems are supposed to provide a long lifetime (>20 years) and, with that, be both cost-effective and environmentally friendly [16]. The sand-blasting used to remove the welding defects on the outer steel formed surface is a convenient surface treatment for the thermal spray arc-wire coating of aluminum. The twin arc-wire system was the PERFECT Spray from SMS Group, Düsseldorf, Germany. The typical conditions for arc spraying were arc parameters of 28 V and 90 A, and a wire speed of 2 m/min. The diameter of the aluminum wire was 1.6 mm. The coating was sprayed uniformly over all of the surface of the outer formed steel sheet.

A black absorbing coating was applied to the outer formed steel sheet by spraying, followed by curing at 300 °C. The benefits of such surfaces are their comparative simplicity to produce and the potential for cost-effectiveness. This novel coating chemistry combines high solar-absorbing performance, high thermal resistance to withstand excessive heat from the metal surface, and good resistance to UV and humid conditions to ensure a long service life. The coating thickness can be controlled in the range of a few micrometers to several tens of microns by using several steps of spraying and drying. The reflectance spectrum of the coating deposited as a solar absorber is presented in Figure 10. The solar absorptance in the UV-VIS-NIR spectra is 95% and can slightly change depending on the surface roughness and the coating thickness. The emissivity of the coating was relatively high, as the solar absorbance was low in the NIR region of the spectrum, leading to the solar absorber exhibiting non-selective behavior.
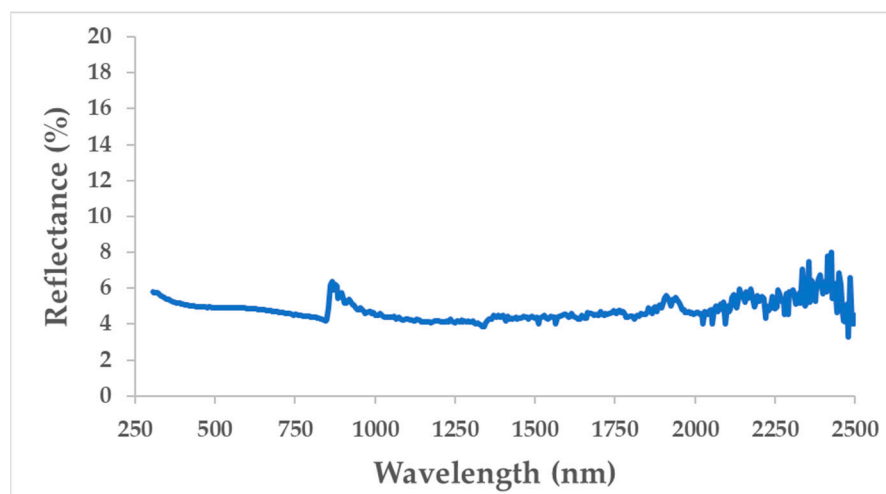

Figure 10. Reflectance spectrum of the silica–carbon sol-gel coating applied as the solar absorber.

2.4. Collector Testing Setup

A solar thermal collector integrating incremental formed panels coated with sol-gel absorbing layers was manufactured for thermal testing. The collector contained eight

panels to generate a surface of 1.6 m², comparable to solar thermal collectors available on the market. Figure 11a shows a view of the rear side of the solar collector as manufactured, while Figure 11b shows the same view with insulation. The insulation material installed on the back of the solar panels was PIR foam boards laminated with aluminum foil, 4 cm thick, from IKO Enertherm (thermal conductivity 0.022 W/m·K). The flexible pipes were insulated with polyethylene slotted-pipe lagging (inner diameter 15 mm, wall thickness 13 mm, and thermal conductivity 0.036 W/m·K). Leakage tests were performed to confirm the quality of the welding and the connections of the flexible fluid pipes.

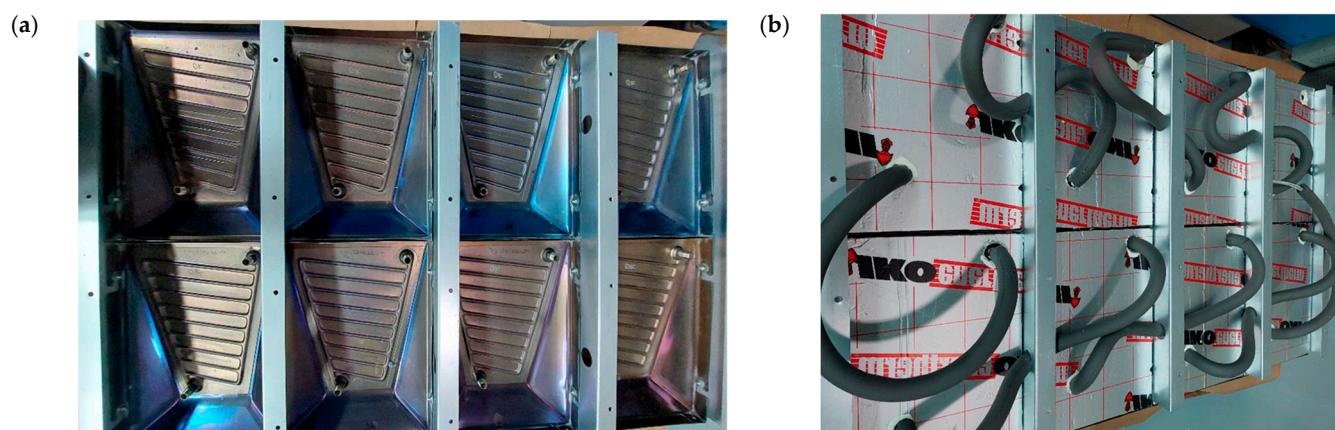(**a**)   (**b**)

Figure 11. Pictures of the solar collector as manufactured without insulation (**a**) and with rear insulation (**b**).

3. Collector Characterization

A schematic diagram of the experimental set-up is presented in Figure 12. This system provides the fluid to the thermal panels via insulated pipes equipped with measurement probes and a circulator. The probes are placed directly at the inlet and outlet of the panel in order to minimize the losses and errors of measurements related to the pipes. The flow rate is adjusted via a manual valve in series on the sample supply circuit. The temperatures are measured at the inlet and outlet of the panel via thermocouples. In order to achieve very good stability for the inlet temperature, the measuring system has a large buffer tank and an internal temperature regulation system. This system is cooled via an external water cooling unit (chiller). The storage tank is equipped with a water-mixing unit to guarantee the homogeneity of the temperature. The heat output of the panel is determined by considering the characteristics of the fluid, the temperature variation, and the flow rate. The thermal conversion efficiencies of the panel are determined by controlling the flux density of the radiation source and knowing the active surface of the panel.
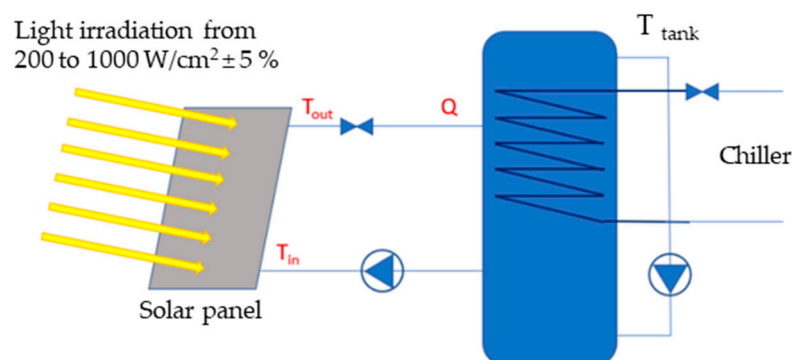

Figure 12. Schematic diagram of experimental test for thermal characterization.

The thermal performance tests were carried out in collaboration with ELIOSYS SA, Liege, Belgium. The investigated heat transfer fluid was water without glycol. As the thermal characteristics of the thermal solar collector were multifactorial, we decided to fix certain parameters. The sample inlet temperature was fixed at room temperature to avoid losses between the pipes and the environment. The measurement of the ambient temperature was carried out in a ventilated enclosure and by obscuring solar irradiance. The measurement time was at least 15 min in steady state. The irradiance measurement was carried out during all tests using a calibrated pyranometer and the thermal environment was controlled by a pyrgeometer. The stability of the irradiation was 0.1% for the duration of the test. Figure 13a shows the experimental setup. Knowing the characteristics of the heat transfer fluid, temperature variations, and flow rate, it was possible to determine the heat output of the system. By controlling the stability of the surface power of the radiation source and knowing the active surface of the sample, it was possible to calculate the thermal conversion efficiencies of the sample. The source of the irradiation was a continuous solar simulator capable of creating irradiation of 200 W/m^2 to 1100 W/m^2 with a maximum variation of less than 1% over 1 h. The spectrum of this simulator was classified B for the wavelength from 800 nm to 900 nm and A for all other wavelengths according to IEC 60904-9 [17].
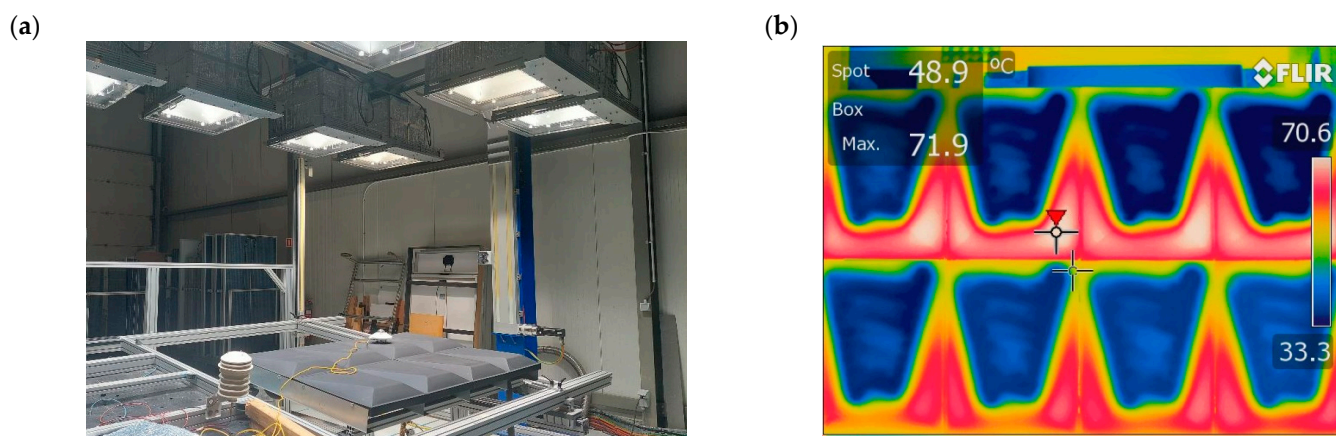
(**a**)

(**b**)

Figure 13. Experimental setup, including the solar collector and irradiance lamps (**a**) and infrared camera image of the solar collector in operation (**b**).

Figure 13b shows an example of thermal imaging, helping to visualize the interconnection of panels. The first panel (top right) was cooler than the last panel in the chain (bottom right). The irradiation power was fixed at 1000 W/m^2 and the water temperature input was fixed at 30 °C +/− 0.2 °C in the panel located at the top-right and exits at the temperature given at the bottom-right. Outside the cooled areas of the panels, a significant increase in temperature was detected, contributed by thermal conduction to the increase in fluid temperature.

3.1. Thermal Power

The thermal power of the collector was determined for various irradiance values (Figure 14a). For a typical irradiance of 1000 W/m^2 and a cooling water flow of 3.7 L/min, the total output power of the collector was 745 W/m^2. This graph also shows that the thermal conversion was better at low irradiance than at high irradiance. This phenomenon was slight and mainly originated from first- and second-order thermal losses, which increased with the temperature difference between the collector and the environment. The tilt angle of the collector significantly influenced the thermal power, as presented in Figure 14b). Indeed, the installation of the collector in a vertical orientation decreased the output power to around 17% compared with the horizontal orientation.
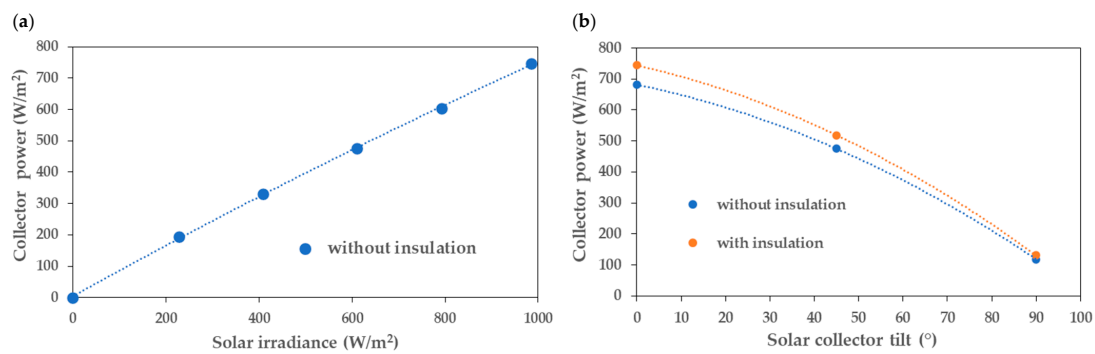
Figure 14. Variation in the thermal power of the collector versus the irradiance for a constant water flow rate of 3.7 L/min (**a**) and variation in the thermal power versus the irradiance angle (**b**).

3.2. Thermal Efficiency

The European standard EN 12975 [18] defines the efficiency η of a thermal collector on the basis of four parameters according to Equations (1) and (2):

$$\eta = \eta_0 \left(\frac{a_1 \cdot \Delta T}{E_0} \right) - \left(\frac{a_2 \cdot \Delta T^2}{E_0} \right) \tag{1}$$

$$\Delta T = T_{water\ out} - T_{water\ in} \tag{2}$$

where:

η—collector efficiency;

η_0—optical efficiency;

a_1 and a_2—heat loss coefficients;

E_0—solar radiation;

ΔT—Temperature difference of the solar fluid between the inlet and outlet of the collector.

The overall efficiency η is, therefore, not a single value, but a characteristic curve. The optical efficiency η_0 represents the maximum efficiency of the thermal collector when the temperature of the fluid is at ambient temperature (no thermal losses). Measured under standardized test conditions (AM1.5 spectrum, solar irradiation E_0 = 1000 W/m^2, perpendicular to the sensor), the efficiency of a thermal collector depends on the properties of the glazing and/or the selectivity of the absorber. Figure 15 shows the variation in the collector efficiency as a function of the flow rate of the cooling fluid. The thermal insulation of the collector slightly influenced its efficiency. On the characteristic curve, the stagnation temperature of the collector was defined as the temperature difference at which the solar gains could not compensate for the thermal losses.
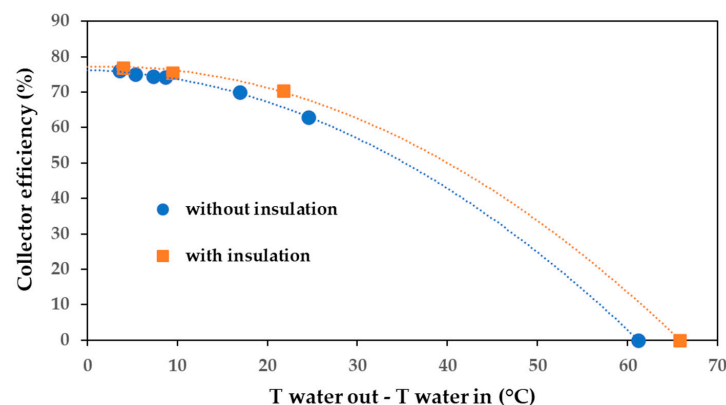

Figure 15. Collector efficiency with and without back insulation for E_0 = 1000 W/m^2.

4. Economic Analysis

An economic feasibility study was carried out to estimate the manufacturing costs of the new type of collector. To show the influence of the forming technology used on the total manufacturing costs, ISF was compared with a conventional deep drawing for quantities n of 1 and 1000 pieces.

The starting point for the cost calculation was the scaled collector geometry shown in Figure 1 and the consideration of the process chain described in Figure 16.
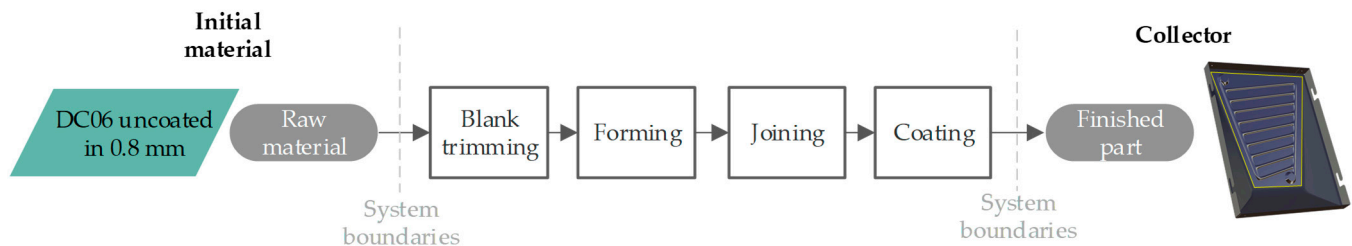

Figure 16. Simplified process chain for the manufacture of the collector.

In this simplified representation of the manufacturing process, the steps of the single-part production of the inner and outer sheets are summarized in the first three superordinate processes of blank trimming, forming, and trimming.

In addition to the main forming costs, the one-time costs for the formation of simulation (deep drawing), as well as the path generation (ISF), are included in the forming process step. All trimming and joining operations were performed using a laser. The coating process itself was divided into the sub-processes of corrosion protection and solar coating.

The assumed boundary conditions and the determined costs for each (sub-)process step are given in Table 1.

Table 1. Boundary conditions and detailed cost distribution by process step for collector-manufacturing depending on the formation technology and quantity *n*.

Process	Sub Process	ISF		Deep Drawing	
		n = 1	*n* = 1000	*n* = 1	*n* = 1000
Raw material (inner + outer sheet)	-	≈16 €		≈16 €	
Forming (inner + outer sheet)	Simulation (one-time)	-		≈800 €	
	Tool-path generation (one time)	≈200 €		-	
	Tooling costs (one time)	≈1500 €		≈20,000 €	
	Manufacturing time per collector	≈2.9 h		≈0.09 h	
	Forming cost per collector	≈292 €		≈22 €	
	Total forming cost per collector	≈2192 €	≈294 €	≈21,622 €	≈43 €
Trimming (inner + outer sheet)	Jig costs (one-time)	≈250 €		≈250 €	
	Laser trimming cost per collector	≈4.20 €		≈4.20 €	
	Total trimming cost per collector	≈254 €	≈5 €	≈254 €	≈5 €
Joining	Total joining cost per collector	≈270 €	≈25 €	≈270 €	≈25 €
Coating	Costs of corrosion protection (Al-Zn)	≈245 €	≈20 €	≈245 €	≈20 €
	Costs of solar coating (sol-gel)	≈37 €	≈17 €	≈37 €	≈17 €
	Total coating cost per collector	≈282 €	≈37 €	≈282 €	≈37 €
Total manufacturing costs per collector		≈3014 €	≈376 €	22,444 €	126 €

The results of the process chain analysis show that the formation and associated tooling investment costs were the drivers for all process variants investigated. As expected, for small quantities, ISF can take advantage of its universal forming stylus and low overall tooling costs. With total manufacturing costs per collector of approx. 3014 € for a quantity of one, the costs of ISF were 87% lower compared with the use of conventional deep-drawing technology. In contrast, deep drawing has advantages for larger quantities due to the significantly short process times. When considering a number of 1000 pieces, the unit price per collector of 126 € for the deep drawing variant was 33% lower than that of the ISF variant. For large quantities, conventional forming is clearly preferable. In the case of prototypes or small quantities, however, ISF is an interesting alternative. In this specific case, the break-even would be at 73 collectors. From this point on, the manufacturing costs for deep drawing are lower than those for ISF.

In view of the large-scale production capability of the collector type presented, the graphical representation of the cost distribution in Table 2 shows that, in addition to formation, coating and joining account for the largest shares in terms of total costs. In the deep drawing scenario at a quantity of n = 1000, the share of formation is approx. 34%, followed by coating (≈29%) and joining (≈20%).

Table 2. Overview of the estimated manufacturing costs per collector depending on the forming technology and quantity *n*.
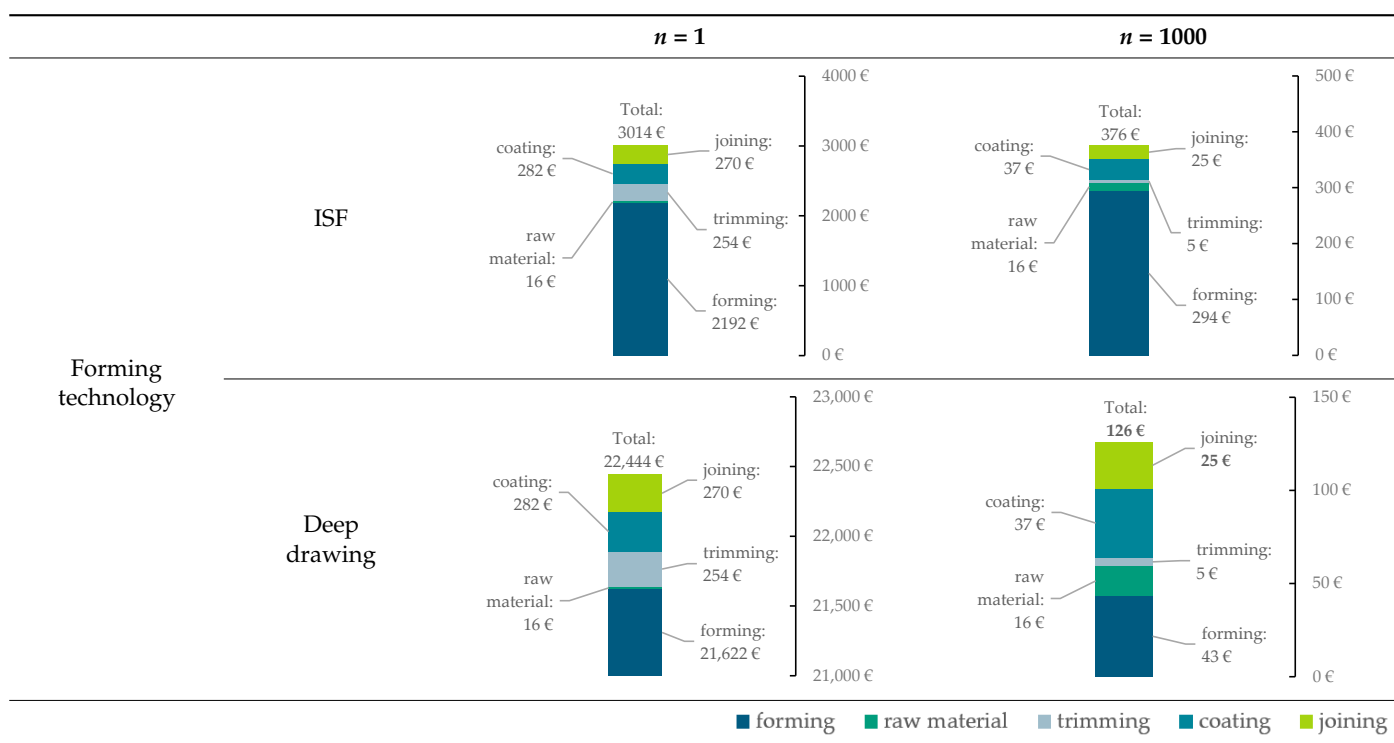
If the costs are related to the collector area, the costs for the new collector type were approx. 625 €/m^2 under the assumptions made. In combination with the degree of design freedom made possible for the first time, the type of collector presented represents an interesting addition and extension to existing systems.

5. Discussion

As shown above, there is good potential for all-sheet metal solar collectors, as the thermal performance and cost were comparable to those of modern flat plate collectors, with the added benefit of three-dimensional design freedom for seamless integration into facade systems.

It was demonstrated that the manufacture of complex collector geometry with the chosen parameters without cracks was possible by ISF. However, as expected, the cost analysis showed that the area of application for this manufacturing technology was only limited to small quantities (e.g., prototypes or individualized elements) due to the long manufacturing time. For large quantities with recurring geometries, it would make more economic sense to use conventional forming technologies with high output rates. The high quantities amortize the initial investment costs in the forming tools and enable low marketable unit costs.

Laser welding was proven to be an efficient method for the assembly of an all-sheet metal collector, despite the 3D complex shape. However, the increase in the metal thickness could considerably improve the welding robustness influenced by sheet formation.

The use of sol-gel painting spray was an efficient and low-cost way to deposit the solar-absorbing layer on a complex-shaped surface. The high solar absorptance and high emissivity of the solar layer could generate a high thermal efficiency of the solar collector at a low temperature. The overheating effect of the present thermal panels was significantly reduced, as the maximum heating temperature was under 100 °C. Indeed, the overheating effect observed in the case of fluid stagnation (e.g., power cut, failure of the primary pump, or when the heat demand is low) for conventional glazed thermal panels using selective absorbing layers generates a high increase in the fluid temperature (>150 °C), leading to premature component degradation. The large surface available for the implementation of these new solar facades, combined with their high efficiency at low temperature, can generate an economical approach to saving energy. However, the coating design could be improved to decrease the surface emissivity and, consequently, to increase the efficiency at higher temperatures; however, this can be achieved only by using complementary antireflective coatings.

6. Conclusions

This project has shown that, within the research project "FutureFacade", new potential for renewable energies in cities can be created. Solar thermal-active facades are particularly suitable for large buildings with large facade areas, as these are the first places where it becomes economically viable.

The approach of using standardized facade substructures was proven successful. However, this project still has a lot of development potential. With regard to the manufacturing process, it is advisable to switch to the more economical manufacturing process for subsequent projects. This would also make the production of smaller facades and quantities more economical. The material could also be changed to aluminum instead of steel in order to minimize the weight of the facade construction. Changes in material and forming technology also allow new design freedom in the geometry of further developed facade panels, which can be further extended by adapting the coating. In terms of appearance, it would be desirable to be able to create more variance in color with the same or similar efficiency. In terms of efficiency, it would also be advisable to further develop the channel structure professionally with the help of meaningful CFD simulations. When considering the efficiency, its ratio with the absorber surface must always be taken into account. With regard to the panel size, adjustments could be made in the future. As long as the absorber surface area is 2 m^2, the collector remains comparable to conventional absorbers.

All in all, the "FutureFacade" approach has brought many new insights and provides new stimuli for further research on solar thermal facades.

Author Contributions: Conceptualization, P.S.; collector design, P.S., D.W., L.S. and M.D. (Martin Dembski); architectural aspects, L.S., M.D. (Martin Dembski) and A.S.; facade construction and integration, L.S. and M.D. (Martin Dembski); incremental forming tests, P.S. and D.W.; joining and coating experiments, F.D. and S.L.C.; collector characterization, F.D. and S.L.C.; economic analysis, P.S. and F.D; resources, J.K., M.D. (Martin Dix) and A.S.; writing—review and editing, P.S., D.W., L.S., M.D. (Martin Dembski), A.S., J.K. and M.D. (Martin Dix). All authors have read and agreed to the published version of the manuscript.

References

1. Bundesregierung. CO_2-Gebäudesanierung. Available online: https://www.bundesregierung.de/breg-de/aktuelles/co2-kohlenstoffdioxid-oder-kohlendioxid-gebaeudesanierung-614754 (accessed on 29 November 2022).
2. International Energy Agency. Technology Roadmap—Energy Efficient Building Envelopes. Available online: https://www.iea.org/reports/technology-roadmap-energy-efficient-building-envelopes (accessed on 29 November 2022).
3. Rynska, E. Review of PV Solar Energy Development 2011–2021 in Central European Countries. *Energies* **2022**, *15*, 8307. [CrossRef]
4. Kaufmann, D. Multifunktionales energieeffizientes Dach- und Fassaden-Solarelement—DAFASOL: Teilvorhaben: Entwicklung des Bauelementes und Anpassung an Einsatzfälle im Stahlbau: Sachbericht: Laufzeit des Vorhabens: 01.12.2014–30.11.2017. Available online: https://www.tib.eu/de/suchen?tx_tibsearch_search%5Baction%5D=download&tx_tibsearch_search%5Bcontroller%5D=Download&tx_tibsearch_search%5Bdocid%5D=TIBKAT%3A1017755027&cHash=ef067e89bb2d1593251944ea0064ceb0#download-mark (accessed on 29 November 2022).
5. Munari-Probst, M.; Roecker, C.; Schueler, A. Architectural integration of solar thermal collectors: Results of a European survey. In Proceedings of the ISES 2005 Solar World Congress, Orlando, FL, USA, 6–12 August 2005.
6. Munari-Probst, M.; Cristina, M.; Roecker, C. *Architectural Integration and Design of Solar Thermal Systems*, 2nd ed.; EPFL Press: Lausanne, France, 2011.
7. Buker, M.S.; Riffat, S.B. Building integrated solar thermal collectors—A review. *Renew. Sustain. Energy Rev.* **2015**, *51*, 327–346. [CrossRef]
8. Hermann, M.; Karin, L.; Hillerns, F. BIONICOL—Entwicklung eines bionischen Solarkollektors mit Aluminium-Rollbond-Absorber. In Proceedings of the 20. Symposium Thermische Solarenergie, Bad Staffelstein, Germany, 5–7 May 2010; pp. 74–79.
9. Tekkaya, E.; Rainer, S. Entwicklung von Solarabsorbern in Stahlbauweise auf Basis partiell plattierter Hybridhalbzeuge. In *Forschung für die Praxis P820*; Verl. und Vertriebsges. mbH: Düsseldorf, Germany, 2015.
10. Maurer, C.; Cappel, C.; Kuhn, T.E. Progress in building integrated solar thermal systems. *Sol. Energy* **2017**, *154*, 158–186. [CrossRef]
11. Schreiber, R.G.; Schaeffer, L. Manufacture of absorber fins for solar collector using incremental sheet forming. *J. Mater. Res. Technol.* **2019**, *8*, 1132–1140. [CrossRef]
12. Weiss, W.; Stadler, I. Facade integration—A new promising opportunity for thermal solar collectors. In *Proceedings of the Industry Workshop of the IEA Solar Heating and Cooling Programme*; Task 26; International Energy Agency: Delft, The Netherlands, 2001.
13. Matuška, T.; Sourek, B. Aspects of solar collector integration into building facade. In Proceedings of the 6th EuroSun, Glasgow, UK, 27–30 June 2006.
14. Behnisch, M.; Münzinger, M.; Poglitsch, H. Die vertikale Stadt als solare Energiequelle? Theoretische Flächenpotenziale für bauwerksintegrierte Photovoltaik und Abschätzung der solaren Einstrahlung. *Transform. Cities* **2020**, *4*, 58–62.
15. Behnisch, M.; Münzinger, M.; Poglitsch, H.; Willenborg, B.; Kolbe, T.H. Anwendungsszenarien von Geomassendaten zur Modellierung von Grünvolumen und Solarflächenpotenzial. In *IÖR Schriften Band 78*; Rhombos Verlag: Berlin, Germany, 2020; pp. 251–261.
16. Knudsen, O.Ø. *Coatings Systems for Long Lifetime: Thermally Sprayed Duplex Systems*; Final Report; SINTEF Rapport: Trondheim, Norway, 2010.

17. *IEC 60904-9:2020*; Photovoltaic Devices—Part 9: Classification of Solar Simulator Characteristics, 3rd ed. IEC Central Office: Geneva, Switzerland, 2020.
18. *DIN EN 12975:2022-06*; Solar Collectors—General Requirements. Beuth Verlag GmbH: Berlin, Germany, 2022. [CrossRef]